Lawrence Berkeley National Laboratory
LBL Publications

Title

Low energy electron attenuation lengths in core—shell nanoparticles

Permalink
https://escholarship.org/uc/item/827766rg

Journal
Physical Chemistry Chemical Physics, 19(20)

ISSN
0956-5000

Authors
Jacobs, Michael I
Kostko, Oleg
Ahmed, Musahid
et al.

Publication Date
2017-05-24

DOI
10.1039/c7cp00663b

Peer reviewed

eScholarship.org Powered by the California Digital Library
University of California

Low Energy Electron Attenuation Lengths in Core-Shell Nanoparticles

Michael I. Jacobs[1,2], Oleg Kostko[2], Musahid Ahmed,[2] Kevin R. Wilson[2,*]

[1]Department of Chemistry, University of California, Berkeley, CA 94720, United States

[2]Chemical Sciences Division, Lawrence Berkeley National Laboratory, Berkeley, CA 94720, United States

* Correspondence to: krwilson@lbl.gov, (510) 495-2474

Abstract:

A velocity map imaging spectrometer is used to measure photoemission from free core-shell nanoparticles, where a salt core is coated with a liquid hydrocarbon shell (i.e. squalane). By varying the radial thickness of the hydrocarbon shell, electron attenuation lengths (EALs) are determined by measuring the decay in photoemission intensity from the salt core. In squalane, electrons with kinetic energy (KE) above 2 eV are found to have EALs of 3-5 nm, whereas electrons with smaller KE (<2 eV) have significantly larger EALs of >15 nm. These results (in the context of other energy-resolved EAL measurements) suggest that the energy dependent behavior of low energy electrons is similar in dielectrics when KE >2 eV. At this energy the EALs do not appear to exhibit strong energy dependence. However, at very low KE (<2 eV), the EALs diverge and appear to be extremely material dependent.

Introduction:

Electrons scatter both elastically and inelastically as they propagate through a material. The inelastic mean free path (IMFP) is the mean distance an electron with a specific kinetic energy (KE) travels between inelastic scattering events.[1] Understanding the energy dependence of the IMFP in materials is important in several different disciplines. For example, the short distance an electron travels between inelastic collisions makes photoelectron spectroscopy a surface sensitive technique.[2,3] If the energy dependence of the IMFP is known, then photoemission experiments can be used to obtain depth-resolved chemical information by varying the photoelectron KE.[4] Likewise, the IMFP of electrons is central to understanding photoemission heating of interstellar dust clouds that arises from the absorption of UV radiation. The magnitude of the electron IMFP is predicted to have a direct effect on the extent of warming.[5] Additionally, inelastic collisions of low energy electrons with DNA produce irreversible, detrimental effects due to bond scission reactions.[6–8] The extent of this damage is dependent on both the electron IMFP in the biological medium as well as the cross sections for the interactions.[9]

Most measurements of the IMFP have been made at high KE by depositing a thin film of material on a substrate and monitoring photoemission from the substrate as a function of film thickness, or by monitoring intensity of backscattered electrons.[10] Measurements of the IMFP of electrons with KE <100 eV in soft materials (such as liquids) are difficult due to experimental challenges (such as high vapor pressures or difficulties collecting all photoelectrons using a hemispherical analyzer). Studies examining the propagation of low KE electrons in materials generally measure the electron attenuation length (EAL). The EAL is the film thickness that results in a $1/e$ decrease in signal intensity at a given energy compared to a non-coated substrate.[1] It is closely related to the IMFP, but because EAL convolutes elastic and inelastic scattering, it is

calculated to be 15-30% shorter (depending on the KE of the electron and material).[1,11] The first low KE EALs measurements were made by impinging electrons onto a thin film and measuring the resulting transmission current.[12–20] These measurements generally resulted in a single "low energy" EAL that was highly material specific (for example, the low energy EALs for pentacene and perylene were reported to be 7.5 and 80 nm, respectively).[20] With the introduction of liquid jet experiments, measurements of the EAL in high vapor pressure liquids (such as water) became possible by either monitoring the angular dependence of photoemission[21,22] or coupling the O1s photoionization cross-section to the signal intensity from liquid water at different energies.[23] Additionally, recent work used the angular distribution of photoemission from free nanoparticles to model low energy electron IMFPs.[24,25] While still somewhat experiment specific, these energy-resolved measurements have yielded EALs that range from 1-5 nm for 1-25 eV KE photoelectrons in water.

Two complementary techniques are typically used to study the properties of low energy electrons in thin films: low energy electron transmission (LEET) and photoelectron transmission.[12] In LEET experiments, thin films are irradiated by electrons and either backscattered electrons or transmission current through the film are detected. In this technique, only the electrons that enter (and not those that exit) the thin film are fully-defined in terms of energy and momentum. Thus, information on an electron's interactions within the film is lost because the measured value is generally a current that is independent of energy. Conversely, photoelectron transmission experiments input low energy electrons into a film via photoemission from a substrate (such as a platinum electrode). The low energy electrons that escape the film into vacuum are then detected.

Recent work has used aerosol photoemission to study surface chemistry[26,27], surface segregation[28,29], and electronic properties of nanoparticles.[24,25,30–32] Many of these studies use a

velocity map imaging (VMI) spectrometer and vacuum ultraviolet light[24–26,30,31,33–35] or X-rays[26,32] from a synchrotron to measure the energy and angular distributions of photoelectrons from free nanoparticles. In this work, we use a VMI spectrometer to measure photoemission from free core-shell nanoparticles and measure the EAL in a liquid hydrocarbon, squalane. By coating squalane onto nanoparticles with a defined photoemission spectrum, we are able to measure the EAL for 1-5 eV photoelectrons. Our measurements, when combined with previous measurements of EAL in covalently-bonded, soft materials, show that the EALs of photoelectrons with >2 eV KE are roughly constant and independent of energy. However, for electrons with KE <2 eV, the behavior of photoelectrons is observed to be material dependent.

Experimental Methods:

Size-selected, core-shell nanoparticles of a specific composition are generated using a method that has been previously described.[36] The experimental setup is shown in Figure 1. Briefly, an aqueous solution of the core material (either potassium iodide or sodium chloride) is first atomized and dried over silica gel to a relative humidity (RH) <15%. This yields a stream of polydisperse, solid particles are then size-selected using a scanning mobility particle sizer (SMPS, TSI Inc.). The core diameters used in this experiment are 100, 150 and 200 nm. After size selection, part of the aerosol flow is sampled by a condensation particle counter (CPC) to monitor particle number concentrations. The remaining flow passes through a charcoal denuder to eliminate any unwanted volatile organic contaminants. The core aerosol is then passed through a tube furnace containing a pyrex tube with the coating material (i.e. liquid squalane). The coating forms on the core via heterogeneous nucleation upon exiting the heated section of the oven. The thickness of the coating is controlled by varying the temperature of the oven, and the size of the core-shell particle is measured using a second SMPS. The coating thickness is determined from the difference

in diameter between aerosol that passes through the furnace and the uncoated aerosol stream that bypasses the oven. Radial coating widths vary from ~1 to 9 nm with roughly ±0.3 nm uncertainties (Figure S4). This treatment assumes that the nanoparticles are spherical, while in reality they most likely exist as rounded cubes. Previous work studying electron impact ionization of organic coated alkali halides using a similar coating technique found the monolayer coating thickness for a liquid hydrocarbon to be ~0.7 nm.[37] Because most measurements reported here have coating thicknesses >0.7 nm, the aerosol particles are assumed to be completely coated. Some systematic errors in the coating thickness could exist due to the non-spherical nature of the particles and the potential for non-uniform coating.

Photoemission from free aerosol particles is measured using a VMI spectrometer (described previously).[26] Three electrodes in the spectrometer are tuned to achieve velocity mapping conditions,[38] where a projection of the nascent velocity distribution of photoelectrons is imaged on a multi-channel plate/phosphor detector with a CMOS camera. Photoelectron images of coated aerosol are collected for 150 s, and sample images at each coating thickness are collected in duplicate. The photoemission images are converted to photoelectron spectra using typical image processing techniques.[39] As shown in Figure 2, the images are asymmetric due to the short absorption length of vacuum ultraviolet light. As has been discussed previously, this leads to preferential photoemission from the front of the nanoparticle and shadowing of the back of the particle.[25,31,33] A discussion of the effect image asymmetry has on the extracted KE spectra is included in the Supplemental Information. Images from the uncoated core are collected after each coating thickness, and the photoelectron spectra from the uncoated core are used to normalize the coated signal for any drifts in instrument or particle generation. Experiments were performed at

112 the Chemical Dynamics Beamline (9.0.2) at the Advanced Light Source, Lawrence Berkeley
113 National Lab.

114 To determine EALs in a coating, squalane is coated onto a KI core and photoemission from
115 the particles is measured as a function of coating thickness. As the coating thickness increases, the
116 intensity of photoemission from the core material decreases due to inelastic collisions. EALs of
117 photoelectrons are determined by tracking the decay of photoemission from the core as a function
118 of coating thickness. KI is chosen as the core material due to its low ionization threshold (6.8 eV)[40]
119 compared to squalane (8.4 eV).[41] Figure 2 shows the KE distribution of photoelectrons from pure,
120 monodispersed KI nanoparticles (diameter, D_p = 150 nm, ~10^4 particles/cm^3) and pure,
121 polydisperse squalane nanoparticles (D_p ~ 220 nm, ~10^6 particles/cm^3). The KE of photoelectrons
122 from KI extends to higher energies than that of squalane due to the difference in threshold energies.
123 The absolute photoemission intensity from squalane is very small compared to that of KI.
124 Measurable photoemission intensities from pure squalane nanoparticles could only be recorded
125 using a polydisperse aerosol distribution, which has ~100x more particles than the size selected KI
126 flow (Figure 2). Since the amount of squalane coating the KI core is only a small fraction of the
127 squalane in the polydisperse flow, photoemission from squalane is not observable in the
128 experiments to determine EAL. Even so, when determining EALs, we only measured KEs that are
129 large enough to ensure there is no photoemission contribution from squalane. To cover a large
130 range of KEs, photoemission from the core shell nanoparticles is measured at five different photon
131 energies: 8.5, 9, 10, 11 and 12 eV. Photoemission at higher photon energies is not collected due to
132 the interference with water vapor (IE = 12.6 eV).

133 **Results and Analysis:**

134 Figure 3a-e shows photoemission from KI nanoparticles as a function of squalane coating
135 thicknesses at incident photon energies of 8.5, 9, 10, 11, and 12 eV. The initial shape of the
136 uncoated photoemission spectrum (black lines in Figure 3) is determined by the photoionization
137 cross-section of KI at these various energies. At the energies used in this study, the photoelectrons
138 originate from the I 5p state.[40] As the coating thickness increases, two things are readily apparent
139 from these spectra: i) the intensity of the signal decreases with increasing coating thickness and ii)
140 there appears to be shift of the peak energy with increasing coating thickness. This first observation
141 is due to the inelastic collisions of electrons inside the squalane shell. The latter observation can
142 be attributed to the production of low KE electrons from inelastic collisions.[12] If electrons don't
143 lose all of their KE when they inelastically collide, they can still escape from the particle. In this
144 case, the intensities at lower energies would appear to decay slower because as the shell thickness
145 increases, a portion of their intensities would come from higher KE electrons that have undergone
146 inelastic collisions. To minimize the effects from the cascade to lower energy, a "top most interval"
147 analysis is employed and only the highest energy electrons (those within ~0.5 eV of the largest KE
148 in the initial spectra) are used to determine EALs. Figure 4 shows the normalized photoemission
149 intensity at 1.1 and 4.4 eV KE from the 8.5 and 12 eV spectra, respectively. If the EAL in squalane
150 was independent of energy, these curves would decay via the same constant.

151 By definition, the EAL is the coating thickness that results in a 1/e decrease in signal
152 compared to an uncoated substrate. Thus, the photoemission intensity from the core at a specific
153 energy, $I(E, d)$, is measured as a function of coating thickness, d:

154 $$I(E,d) = I(E,0)\, e^{-\frac{y_e(d)}{L_e(E)}}, \quad (1)$$

where $I(E, 0)$ is the initial photoemission intensity at energy, E, without any coating, $y_e(d)$ is the distance the electron must travel through at a given coating thickness, and $L_e(E)$ is the EAL at energy E. As the coating thickness increases, an increasing amount of the incident light is absorbed by the coating. Thus, Eq. 1 is modified to include the decrease in photon intensity that reaches the core due to the increased coating absorption:

$$I(E,d) = \left[I(E,0)e^{-\frac{y_v(d)}{L_v}}\right]e^{-\frac{y_e(d)}{L_e(E)}}. \quad (2)$$

In Eq. 2, L_v is the attenuation length of light in the coating and $y_v(d)$ is distance light travels through at a given coating thickness before encountering the core. At a given photon energy, L_v is equal to $\lambda/4\pi\kappa$, where λ is the wavelength of the incident light and κ is the imaginary component of the refractive index of the coating material. Table S1 shows the energy-dependent κ values of squalane and the associated attenuation length of light, L_v, at the energies we measured.[42] While uncertainties in κ values used in this study were not reported,[42] as will be discussed later, the calculated absorption lengths are generally larger than the measured EALs, which makes Eq. 2 insensitive to changes in L_v.

For the case of a flat surface, the escape length of electrons and penetration length of light is equal to the coating thickness (i.e. $y_v(d) = y_e(d) = d$). Surface curvature has previously been used to explain photoemission from nanoparticles[33] and electron impact charging of nanoparticles.[37] Because the thickness of the shell is much smaller than the particle radius, surface curvature is negligible on the scale of electron scattering and coating thickness closely resembles the overlayer thickness in the EAL definition. Thus, the radial coating thickness (d) is used to describe distance electrons must escape at each shell thickness. However, as shown in Figure 5, the distance the photon travels through the coating will only be equal to the coating thickness when the photon

enters the core shell nanoparticle normal to its surface. From the geometries shown in Figure 5, it can be shown that the distance a photon must travel through the coating to reach the core, $y(d, \theta)$, is:

$$y(d,\theta) = (R + d)\cos[\beta(\theta)] - \sqrt{R^2 - (R + d)^2 \sin^2[\beta(\theta)]}, \tag{3}$$

where R is the radius of the core and $\beta(\theta)$ is the refracted angle between the incident light and the particle surface. The refracted angle is determined using Snell's law with the previously measured refractive indices in squalane.[42] Previous work by Ziemann *et al.*[37] has shown that the probability, $g(\theta)\mathrm{d}\theta$, a photon enters the particle at an angle between θ and $\mathrm{d}\theta$ is:

$$g(\theta)d(\theta) = 2\pi h\,\mathrm{d}h/\pi R^2 = 2\sin\theta\cos\theta\,\mathrm{d}\theta, \tag{4}$$

where h is defined in Figure 5. The average attenuation of light as it travels through the coating, $\langle e^{-\frac{y_v(d)}{L_v}} \rangle$, before striking the core is given by:

$$\langle e^{-\frac{y_v(d)}{L_v}} \rangle = \int_0^{\pi/2} e^{\frac{y(d,\theta)}{L_v}}\,\mathrm{g}(\theta)\,d\theta. \tag{5}$$

This integral does not have an exact solution and is solved numerically at each coating thickness. EALs are determined by using Eq. 5 to describe $\langle e^{-\frac{y_v(d)}{L_v}} \rangle$ and fitting the normalized intensity plots (e.g. Figure 4) at each KE to the following:

$$\frac{I(E,d)}{I_0(E,0)} = \alpha\,\langle e^{-\frac{y_v(d)}{L_v}} \rangle\, e^{-\frac{d}{L_e(E)}}, \tag{6}$$

where α is a fitting parameter that is constrained to be less than one.[14] As the core particles are coated by a squalane shell, there is some probability that electrons can be scattered back into the core. Thus, the intensity from the uncoated aerosol is not used in the fit, and α accounts for the diminished number of electrons that enter the shell due to interfacial scattering (Figure 4).

The EALs calculated from the five different photon energies are given in Table 1. This energy range provides measurements of electron attenuation from electrons with 1.1 to 4.4 eV KE. In general, at KE >2 eV, the EAL is determined to be 3-5 nm and does not appear to be a strong function of energy. At lower KE, the EAL increases, and at KE <2 eV, it is >15 nm.

Because the uncertainties in κ are not previously reported,[42] the sensitivity of Eq. 6 to changes in the attenuation length of light was evaluated by applying a ±20% error to κ and determining the resulting change in computed EALs. At a photon energy of 11 eV, the EAL of electrons with 3.4±0.2 eV KE was calculated to be 3.8±1.0 nm using $\kappa = 0.7$ and $L_v = 12.8$ nm. If κ changes to 0.56 and 0.84 (a -20% and +20% error), the measured EAL at 3.4 eV changes to 3.5 and 4.0 nm, respectively. These differences are smaller than the uncertainty in the original measurement and show that the model does not have a strong sensitivity to changes in κ because the EAL is generally significantly shorter than L_v.

Furthermore, because the dimensions of the particle are on the order of the wavelength of light, an accurate description of the intensity in the core would require full Mie scattering calculations. To provide a minimum for the reported EALs, we removed the absorption of light by the shell (i.e. constrained $\langle e^{-\frac{y_v(d)}{L_v}} \rangle = 1$ in Eq. 6), and assumed the attenuation of signal with increased coating thicknesses arose only from inelastic scattering of electrons. This treatment had the result of lowering the EALs by roughly 20-30% and represents a potential systematic error from the data analysis.

Finally, to confirm the measured EAL are specific to the squalane coating and are not dependent on the experimental approach, the size and material of the core were varied. Table S3 shows the EALs in squalane measured with different sized KI cores (100 nm, 150 nm and 200

219 nm). Additionally, Table S2 shows the EALs in squalane using both a KI and NaCl core. While
220 the NaCl photoemission spectra are slightly complicated by squalane photoemission (the
221 ionization thresholds of KI, NaCl and squalane are 6.8, 8.2 and 8.4 eV, respectively),[40,41] the
222 general agreement in escape lengths suggests the observed EALs are specific to the properties of
223 the squalane shell.

224 **Discussion:**

225 The EALs in squalane measured in this study range from 3.3 nm at 4.4 eV to 15.6 nm at
226 1.1 eV. As shown in Table 1, the EALs are roughly constant (~3-5 nm) when KE >2 eV. However,
227 when KE <3 eV, the attenuation lengths increase to >15 nm. Low energy EALs in solid organic
228 films have previously been measured by monitoring electron transmission currents through films
229 of different thicknesses.[13–17,19,43] Energy-resolved EALs in n-$C_{36}H_{74}$ were collected by scanning
230 the incident photon energy on a Pt substrate and changing the film thickness (data shown in Figure
231 6).[16,17] The measured attenuation lengths of 2-5 eV electrons in n-$C_{36}H_{74}$ are ~3-5 nm, which are
232 in good agreement with the attenuation lengths reported here for squalane (also 3-5 nm for a similar
233 energy range). However, when the KE is <2 eV, the EALs in n-$C_{36}H_{74}$ remain constant (~2.5 nm),[16]
234 which differs from the measurements for squalane reported here. At low photoelectron energies,
235 Pfluger *et al.* describe phonon excitation associated with the C-H stretching mode as the primary
236 energy-loss scattering source.[19] However, Cartier *et al.* mention that at lower KE, the measured
237 EALs varied with experimental conditions and the length of time a sample was irradiated due to a
238 changing number of trap states.[16] Because the VMI spectrometer constantly probes a new surface,
239 we don't expect a similar "history" effect in our experiments. The first studies looking at
240 transmission of low energy electrons through organic films were not energy-resolved, and thus
241 only an average "low energy" (<3 eV) EAL was measured. The reported attenuation lengths

242 (generally 10-100s of Å) are extremely dependent on film composition.[13–15,20,43] For example, low
243 energy electrons (<3 eV) had EALs of 7.5 and 80 nm in films composed of pentacene and perylene,
244 respectively.[20] Additionally, experiments looking at low energy electron transmission in methane[44]
245 and krypton[45] films show IMFPs (and thus EALs) that increase at electron KE <2 eV (from 2 nm
246 at 3 eV to 5 nm at 1.7 eV). These studies suggest that at lower KE, there is a corresponding lower
247 density of states and thus fewer possible modes to deposit energy in a given scattering event. Thus,
248 based on the large variability of previously reported EALs, the low KE (<3 eV) EAL appear to be
249 extremely sensitive to the electronic structure of the material.

250 A very recent study also examined the photoemission from core-shell nanoparticles and
251 estimated the EAL of 0.5-1.0 eV photoelectrons using a total electron yield (TEY) measurement.
252 For thin and thick shells of squalane, they report EALs of 8.0±0.5 and 30±3 nm, respectively.[46]
253 The EALs reported here at a similar energy range (15.6 nm for 1.1±0.2 eV electrons) are slightly
254 larger. For a direct comparison with these previous results, TEY of the core is measured as a
255 function of coating thickness at each photon energy. Because TEY combines the photoemission
256 intensity of many different KEs, EALs cannot be directly extracted from this measurement.
257 Instead, the decrease in TEY signal is fit to Eq. 6 to determine an average attenuation coefficient.
258 The average attenuation coefficients are presented in the Supporting Information (Table S3). The
259 work of Amanatidis *et al.* uses a two, 266-nm photon ionization scheme, which results in ~9.3 eV
260 radiation. The core material (sodium benzoate) used by Amanatidis *et al.* has a different ionization
261 threshold (~7.5 eV)[46] than the KI core here (6.8 eV).[40] Thus, the TEY measurements at the specific
262 photon energies are not directly comparable because the KE of the photoelectrons differ. However,
263 the TEY measurements at 8.5 and 9 eV (which result in a KE spectra closest to that of Amanatidis
264 *et al.*) yield average electron attenuation coefficients of 18.8±5.1 nm and 4.9±1.8 nm, respectively.

These average attenuation coefficients bound those reported by Amanatidis *et al*. and suggest the TEY measurements are very sensitive to the incident photon energy.

As a further means of comparison, there is an increasing body of evidence suggesting the EAL in liquid water approaches a constant value at low KEs.[21–23,47] The lowest energy EAL reported by Suzuki *et al*.[23] (3.02 ± 0.46 nm at 5 eV) as well as that reported by Buchner *et al.*[47] (5 nm at 4.65 eV) are in reasonable agreement with the measurements reported here. Additionally, recent work by Signorell *et al.* using angle resolved photoelectron spectroscopy of aqueous nanoparticles extracted the IMPF and EAL of low kinetic energy photoelectrons.[25] The EAL of electrons with 3 eV KE in water is reported to be 3.9 nm, which is in good agreement with the results reported here. However, at lower KEs (<3 eV), Signorell *et al.* reports a decrease in the EAL, which is attributed to an increase in purely vibrational scattering.[25]

Shown in Figure 6 is a comparison of previously published energy-resolved EAL (and IMFP) measurements for covalently bonded, soft materials and water. Shown in this Figure are EALs (up to 25 eV) for carbon containing species,[16,44,46,48] liquid water[22,23,25,47] and solid water.[49] As noted above, there is significant scatter in measurements of the EAL at very low KE (<2 eV) where the EALs are expected to be much more material specific. However, a common feature for all measurements is the consistency of EALs for electrons with >2 eV KE. This is in contrast with the models for electron IMFP and EAL which predict both values to monotonically increase after reaching a minimum at 50-200 eV.[2,3] Based on the results shown in Figure 6, it appears that (to some extent) low KE electrons in covalently bonded, soft materials have equally short EALs and are as surface sensitive as electrons with larger KE. These results have consequences for future photoemission experiments that utilize electron KE to obtain depth profiles. For example, these data suggest that depth profiling photoemission experiments most likely cannot be performed by

288 moving the KE of photoelectrons to lower energy without explicitly measuring the energy
289 dependence of very low KE photoelectrons.

290 **Conclusion:**

291 In this paper, we have used a VMI spectrometer to probe photoemission from free core-
292 shell nanoparticles. The VMI spectrometer detects all electrons that are emitted from the
293 nanoparticles. By changing the thickness of the shell we have determined the low energy EAL in
294 squalane. At very low kinetic energy (<2 eV), the EAL in squalane is >15 nm. At slightly larger
295 kinetic energies (>2 eV), the EAL drops to 3-5 nm. Together with other energy resolved EALs in
296 covalently bonded materials, these results suggest that the attenuation lengths of electrons with >2
297 eV KE do not change with increasing kinetic energy. This finding suggests that these low energy
298 electrons are equally surface sensitive as higher KE photoelectrons. The energy dependence of
299 EALs for electrons with KE <2 eV appear to be highly material specific.

300 The use of core shell aerosol particles to determine EALs is limited when performed using
301 VUV radiation (due to the absorption of light by the shell material). However, this technique
302 appears to have more promise and applicability at higher energies (such as soft X-rays) where the
303 light penetration lengths are larger (i.e. light absorption by the shell can be neglected) and the
304 spectral features (core-shell excitation) are more defined.

305 **Acknowledgments:**

306 This work and the Advanced Light Source were supported by the Director, Office of
307 Energy Research, Office of Basic Energy Science of the U.S. Department of Energy under
308 Contract No. DE-AC02-05CH11231. M.I.J. thanks the NSF for an NSF Graduate Research

Fellowship under DGE-1106400. K.R.W. was supported by the Department of Energy, Office of Science Early Career Research Program.

References:

1 A. Jablonski and C. J. Powell, *J. Electron Spectros. Relat. Phenomena*, 1999, **100**, 137–160.

2 M. P. Seah and W. A. Dench, *Surf. Interface Anal.*, 1979, **1**, 2–11.

3 S. Tanuma, C. J. Powell and D. R. Penn, *Surf. interface Anal.*, 1994, **21**, 165–176.

4 S. Ghosal, J. C. Hemminger, H. Bluhm, B. S. Mun, E. L. D. Hebenstreir, G. Ketteler, D. F. Ogletree, F. G. Requejo and M. Salmeron, *Science (80-.).*, 2005, **307**, 563–566.

5 J. C. Weingartner and B. T. Draine, *Astrophys. J. Suppl. Ser.*, 2001, **134**, 263–281.

6 F. Martin, P. D. Burrow, Z. Cai, P. Cloutier, D. Hunting and L. Sanche, *Phys. Rev. Lett.*, 2004, **93**, 6–9.

7 L. G. Caron and L. Sanche, *Phys. Rev. Lett.*, 2003, **91**, 113201.

8 B. Boudaiffa, P. Cloutier, D. Hunting, M. A. Huels and L. Sanche, *Science (80-.).*, 2000, **287**, 1658–1660.

9 E. Alizadeh, T. M. Orlando and L. Sanche, *Annu. Rev. Phys. Chem.*, 2015, **66**, 379–398.

10 C. J. Powell and A. Jablonski, *J. Phys. Chem. Ref. Data*, 1999, **28**, 19.

11 C. J. Powell, *J. Electron Spectros. Relat. Phenomena*, 1988, **47**, 197–214.

12 R. Naaman and L. Sanche, *Chem. Rev.*, 2007, **107**, 1553–1579.

13 W. B. Berry, *J. Electrochem. Soc.*, 1971, **118**, 597–600.

14 Y. C. Chang and W. B. Berry, *J. Chem. Phys.*, 1974, **61**, 2727.

15 J.-T. J. Huang and J. L. Magee, *J. Chem. Phys.*, 1974, **61**, 2736.

16 E. Cartier, P. Pfluger, J. J. Pireaux and M. Rei Vilar, *Appl. Phys. A Solids Surfaces*, 1987, **44**, 43–53.

17 E. Cartier and P. Pfluger, *Phys. Rev. B*, 1986, **34**, 8822–8827.

18 M. Rei Vilar, M. Schott and P. Pfluger, *J. Chem. Phys.*, 1990, **92**, 5722–5730.

19 P. Pfluger, H. R. Zeller and J. Bernasconi, *Phys. Rev. Lett.*, 1984, **53**, 94–97.

20 S. Hino, N. Sato and H. Inokuchi, *Chem. Phys. Lett.*, 1976, **37**, 494–498.

21 N. Ottosson, M. Faubel, S. E. Bradforth, P. Jungwirth and B. Winter, *J. Electron Spectros. Relat. Phenomena*, 2010, **177**, 60–70.

22 S. Thürmer, R. Seidel, M. Faubel, W. Eberhardt, J. C. Hemminger, S. E. Bradforth and B.

Winter, *Phys. Rev. Lett.*, 2013, **111**, 1–5.

23 Y. I. Suzuki, K. Nishizawa, N. Kurahashi and T. Suzuki, *Phys. Rev. E - Stat. Nonlinear, Soft Matter Phys.*, 2014, **90**, 1–5.

24 M. Goldmann, J. Miguel-Sánchez, A. H. C. West, B. L. Yoder and R. Signorell, *J. Chem. Phys.*, 2015, **142**.

25 R. Signorell, M. Goldmann, B. L. Yoder, A. Bodi, E. Chasovskikh, L. Lang and D. Luckhaus, *Chem. Phys. Lett.*, 2016, **658**, 1–6.

26 M. I. Jacobs, B. Xu, O. Kostko, N. Heine, M. Ahmed and K. R. Wilson, *J. Phys. Chem. A*, 2016, **120**, 8645–8656.

27 F.-X. Ouf, P. Parent, C. Laffon, I. Marhaba, D. Ferry, B. Marcillaud, E. Antonsson, S. Benkoula, X.-J. Liu, C. Nicolas, E. Robert, M. Patanen, F.-A. Barreda, O. Sublemontier, A. Coppalle, J. Yon, F. Miserque, T. Mostefaoui, T. Z. Regier, J.-B. A. Mitchell and C. Miron, *Sci. Rep.*, 2016, **6**, 36495.

28 E. Antonsson, M. Patanen, C. Nicolas, J. J. Neville, S. Benkoula, A. Goel and C. Miron, *Phys. Rev. X*, 2015, **5**, 11025.

29 P.-C. Lin, Z.-H. Wu, M.-S. Chen, Y.-L. Li, W.-R. Chen, T.-P. Huang, Y. Lee and C. C. Wang, *J. Phys. Chem. B*, 2017.

30 K. R. Wilson, D. S. Peterka, M. Jimenez-Cruz, S. R. Leone and M. Ahmed, *Phys. Chem. Chem. Phys.*, 2006, **8**, 1884–1890.

31 K. R. Wilson, S. Zou, J. Shu, E. Rühl, S. R. Leone, G. C. Schatz and M. Ahmed, *Nano Lett.*, 2007, **7**, 2014–19.

32 B. Xu, M. I. Jacobs, O. Kostko and M. Ahmed, *ChemPhysChem*, 2017.

33 M. J. Berg, K. R. Wilson, C. M. Sorensen, A. Chakrabarti and M. Ahmed, *J. Quant. Spectrosc. Radiat. Transf.*, 2012, **113**, 259–265.

34 A. H. C. West, B. L. Yoder and R. Signorell, *J. Phys. Chem. A*, 2013, **117**, 13326–13335.

35 K. R. Wilson, H. Bluhm and M. Ahmed, in *Fundamentals and Applications in Aerosol Spectroscopy*, eds. R. Signorell and J. P. Reid, CRC Press, 2011, pp. 367–400.

36 L. Lee and K. Wilson, *J. Phys. Chem. A*, 2016, acs.jpca.6b05285.

37 P. J. Ziemann, P. Liu, D. B. Kittelson and P. H. McMurry, *J. Phys. Chem.*, 1995, **99**, 5126–5138.

38 A. T. J. B. Eppink and D. H. Parker, *Rev Sci Instrum*, 1997, **68**, 3477–84.

39 V. Dribinski, A. Ossadtchi, V. a. Mandelshtam and H. Reisler, *Rev. Sci. Instrum.*, 2002, **73**, 2634.

40 R. Poole, J. Jenkin, J. Liesegang and R. Leckey, *Phys. Rev. B*, 1975, **11**, 5179–5189.

41 H. Koizumi, *Chem. Phys. Lett.*, 1994, **219**, 137–142.

42 L. R. Painter, J. S. Attrey, H. H. Hubbell and R. D. Birkhoff, *J. Appl. Phys.*, 1984, **55**, 756.

43 S. Hino, *J. Chem. Phys.*, 1977, **67**, 4139.

44 J.-P. Jay-Gerin, B. Plenkiewicz, P. Plenkiewicz, G. Perluzzo and L. Sanche, *Solid State Communitcations*, 1985, **55**, 1115–1118.

45 E. Keszei, R. Marsolais, M. Deschenes, T. Goulet, L. Sanche and J.-P. Jay-Gerin, *J. Electron Spectros. Relat. Phenomena*, 1985, **36**, 269–279.

46 S. Amanatidis, B. L. Yoder and R. Signorell, *arXiv:1702.07865 [cond-mat.soft]*.

47 F. Buchner, T. Schultz and A. Lübcke, *Phys. Chem. Chem. Phys.*, 2012, **14**, 5837–42.

48 C. Martin, E. T. Arakawa, T. A. Callcott and R. J. Warmick, *J. Electron Spectros. Relat. Phenomena*, 1986, **42**, 171–175.

49 M. Michaud and L. Sanche, *Phys. Rev. A*, 1987, **36**, 4672–4683.

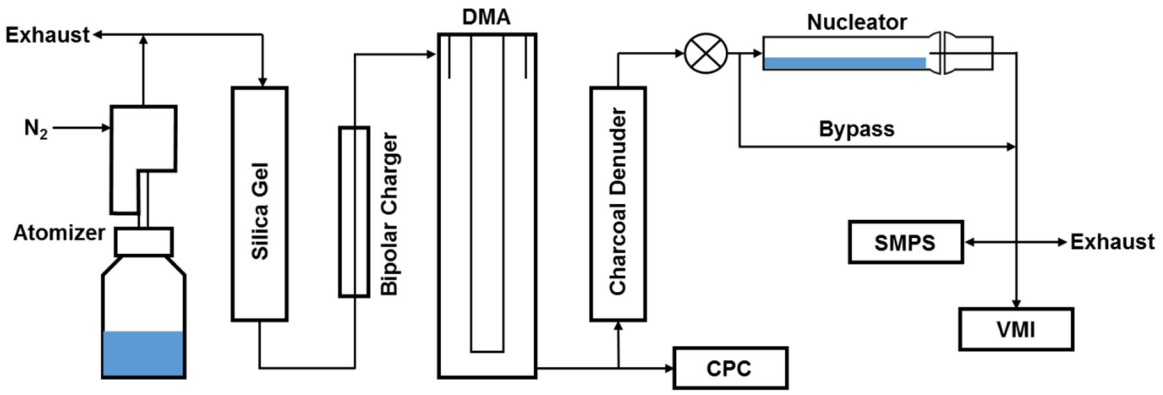

Figure 1. Schematic of the coating experimental setup. (DMA = Differential Mobility Analyzer, CPC = Condensation Particle Counter, SMPS = Scanning Mobility Particle Sizer, VMI = Velocity Map Imaging spectrometer).

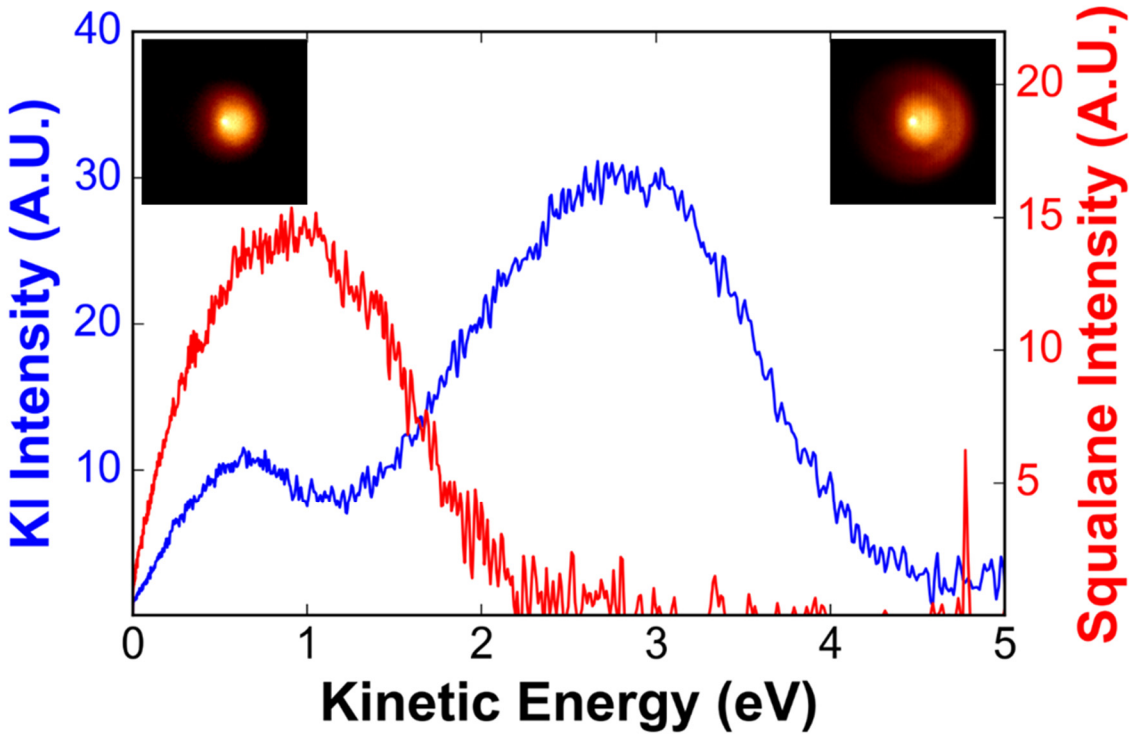

Figure 2. Photoemission spectra of monodispersed KI and polydisperse squalane nanoparticles. The incident photon energy is 11 eV. The insets on the left and right show the images that correspond to the squalane and KI photoemission spectra, respectively. Despite similar intensities, the squalane nanoparticle spectrum is obtained using ~100x more material than the KI nanoparticle spectrum. Because squalane has a lower ionization cross-section and a higher threshold energy than KI, squalane photoemission does not interfere with the decay of KI photoemission intensity at the higher KEs.

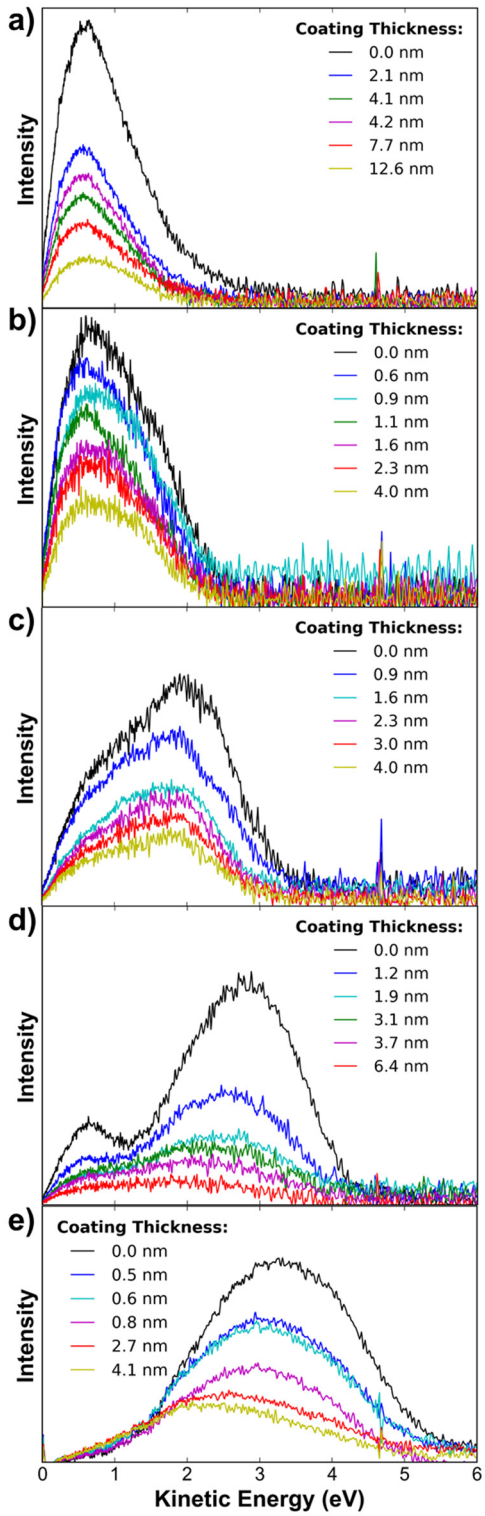

Figure 3. Photoemission spectra of KI-squalane core-shell nanoparticles with varying squalane shell thicknesses. Spectra were collected at incident photon energies of 8.5 eV (a), 9 eV (b), 10 eV (c), 11 eV (d), and 12 eV (e). Note: The side band is missing in the 12 eV spectrum due to large gas phase background at low KE caused by higher harmonics from beamline 9.0.2.

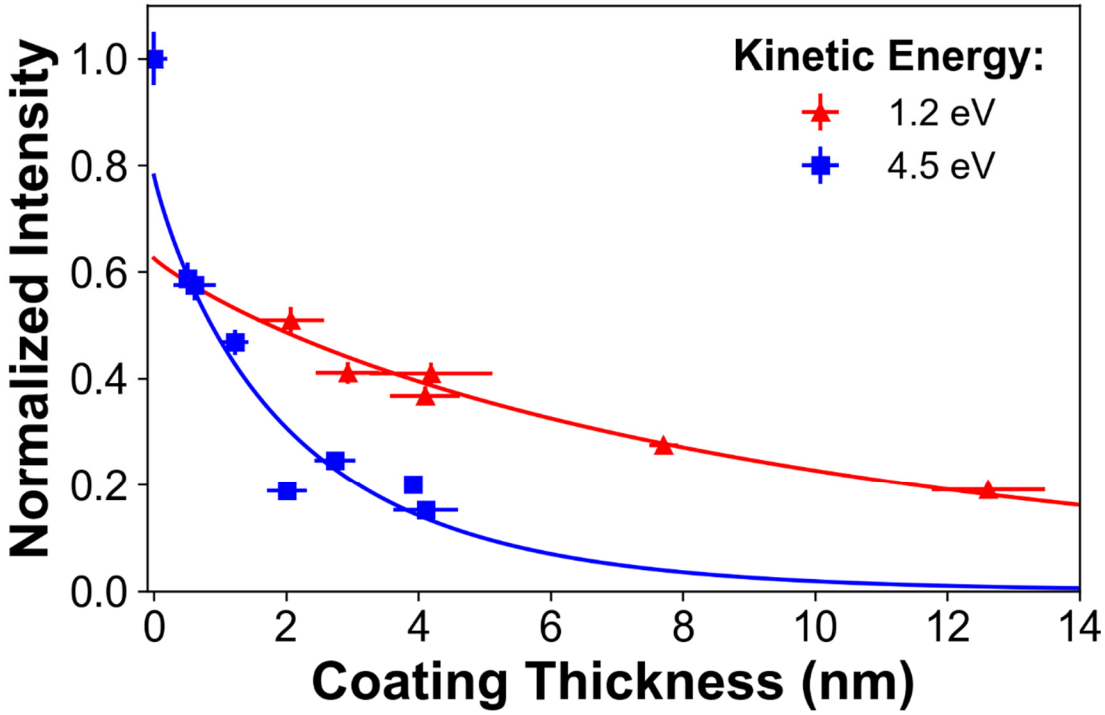

Figure 4. Normalized intensity at 1.1 and 4.4 KE from the 8.5 and 12 eV photoemission spectra, respectively. EAL are extracted from the decay of KI photoemission intensity at different KEs using Eq. 6. An energy dependence in the EAL in squalane results in differences in the decay rates at different KEs.

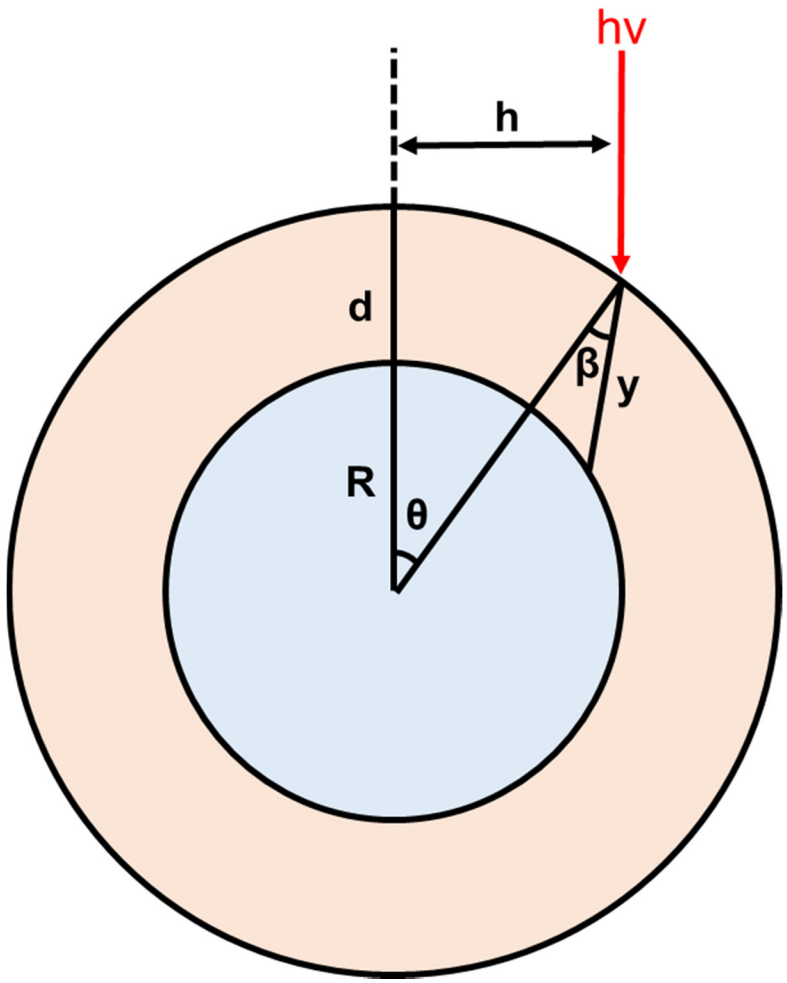

Figure 5. Diagram showing the geometry of light entering the core through the squalane layer.

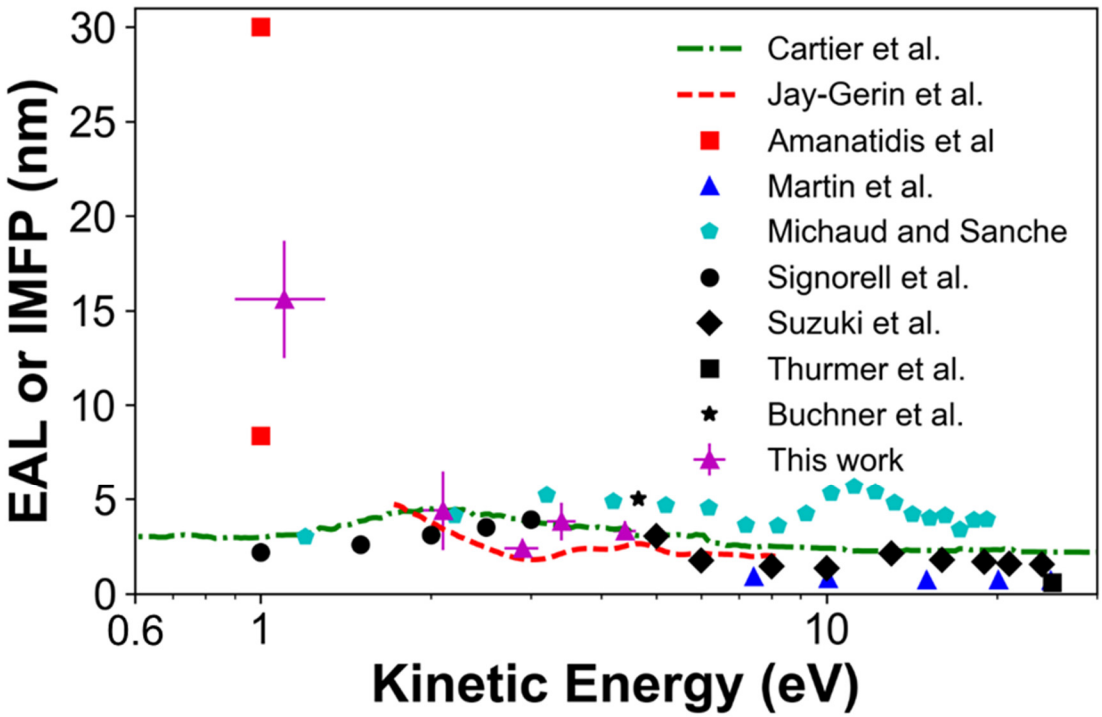

Figure 6. Collection of energy-resolved, low energy EAL in soft materials. The measurements from this work are given by the magenta triangles. Error bars represent ±1s. The green and red dashed lines represent EALs in paraffin, n-$C_{36}H_{74}$ (Cartier et al.[16,17]) and IMFPs in methane (Jay-Gerin et al.[45]) films, respectively. The red squares represent the EAL in thick (top) and thin (bottom) squalane layers (Amanatidis et al.[46]). The blue triangles represent EALs measured in a free standing carbon film (Martin et al.[48]). The black symbols represent EALs in liquid water from aerosol particles (circles, Signorell et al.[25]) and liquid jets (diamonds, Suzuki et al.[23]; square, Thurmer et al.[22]; star, Buchner et al.[47]). The pentagons represent EALs in solid water (Michaud and Sanche[49]). At energies >2 eV, the EAL all remain fairly constant.

Kinetic Energy (eV)	EAL (nm)
1.1±0.2	15.6±3.1
2.1±0.2	4.4±2.1
2.9±0.2	2.4±0.4
3.4±0.2	3.8±1.0
4.4±0.2	3.3±0.4

Table 1. Experimental measurement of the energy dependence of the EAL in squalane. The errors represent uncertainties in the fit to Eq. 6 (±1s). Possible systematic errors are discussed in the text.

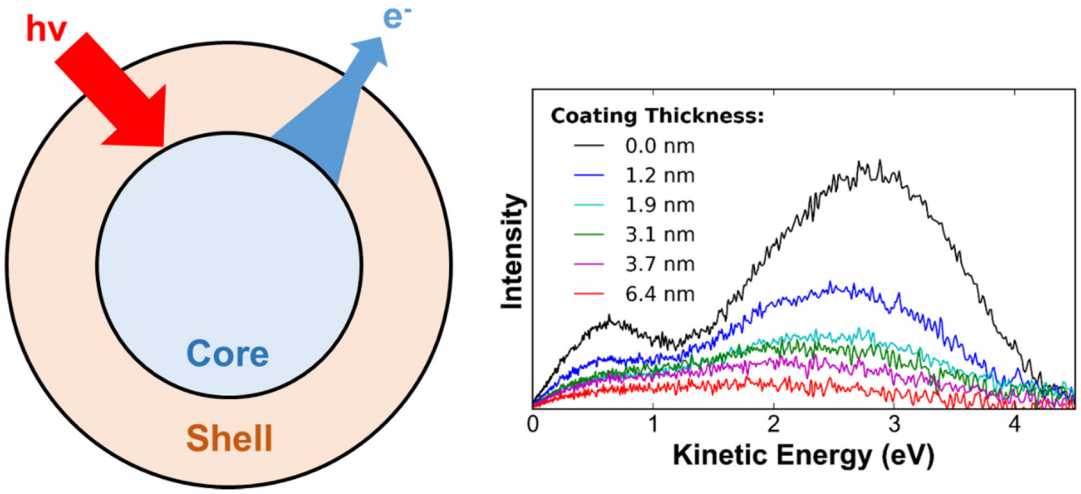
hv
e-
Core
Shell
Coating Thickness:
0.0 nm
1.2 nm
1.9 nm
3.1 nm
3.7 nm
6.4 nm
Intensity
0
1
2
3
4
Kinetic Energy (eV)

TOC Graphic